http://dx.doi.org/10.5012/bkcs.2011.32.9.3338

Structural and Spectroscopic Investigation of Ceria Nanofibers Fabricated by Electrospinning Process

Ah Reum Hwang, Juyun Park, and Yong-Cheol Kang*

*Department of Chemistry, Pukyong National University, Busan 608-737, Korea. *E-mail: yckang@pknu.ac.kr*
Received June 16, 2011, Accepted July 25, 2011

We fabricated ceria (CeO_2) nanofibers by applying a mixed solution of polyvinylpyrrolidone (PVP) and various concentrations of cerium nitrate hydrate ($Ce(NO_3)_3$) ranging from 15.0 to 26.0 wt % by the electrospinning process. Ceria nanofibers were obtained after calcining PVP/$Ce(NO_3)_3$ nanofiber composites at 873 and 1173 K. The SEM images indicated that the diameters of CeO_2 nanofibers calcined at 873 and 1173 K were smaller than those of nanofibers obtained at RT. As the amount of cerium increased, the diameter of CeO_2 nanofibers increased. XRD analysis revealed that the ceria nanofibers were in cubic form. TEM results revealed that the ceria nanofibers were formed by the interconnection of Ce oxide nanoparticles. The ceria nanofibers obtained at low concentrations of Ce (CeL) showed spotty ring patterns indicated that the ceria nanofibers were polycrystalline structure. And the ceria nanofibers obtained at high concentration of Ce (CeH) showed fcc (001) diffraction pattern. XPS study indicated that the oxidation of Ce shifted from Ce^{3+} to Ce^{4+} as the calcination temperature increased.

Key Words : Ceria, Nanofiber, XPS, TEM

Introduction

Recently, nanotechnology has been a big issue throughout the science community. Production of nanofibers is considered as a part of nanotechnology. Electrospinning has been used as a simple and useful method for synthesizing nanosized materials such as nanomats,[1] nanobelts,[2] nanospring,[3] and nanofibers.[4] This technique creates a high specific surface area to volume ratio, high porosity and continuous fibers.[5] Nanofibers have various applications including textile devices,[6,7] catalysts,[8,9] membranes,[10] sensors,[11] biomedical applications,[7,12] and filtration.[11-14] The combination of sol-gel and electrospinning process is the most promising technology for the fabrication of nanofibers.[15]

Nano-sized CeO_2 is used in many applications like cosmetic materials, high-storage capacitor devices,[16] buffer layers for conductors,[17-19] fuel cells,[20,21] and optical devices.[22-24] Also cerium dioxide has been popularly used in automotive catalysts[16,25] because of its unique characteristic of Ce(IV) and Ce (III) converting to one another.[26]

Barreca *et al.* studied the oxidation states of Ce in CeO_2 thin films obtained by plasma-enhanced chemical vapor deposition (PECVD) using XPS.[17] They showed that the obtained CeO_{2-x} films had a tunable Ce^{4+}/Ce^{3+} ratio as a function of the substrate temperature or the O_2 partial pressure. Muroga *et al.* investigated CeO_2 thin films, which are deposited by pulsed laser deposition method on $Gd_2Zr_2O_7$ tapes, by means of SEM and TEM.[18] They revealed that the degree of grain alignment improved as the thickness of CeO_2 film increased. Kanakaraju *et al.* focused on the optical and structural properties of CeO_2 films. The films were deposited through reactive ion beam sputtering technique at different substrate temperatures and oxygen partial pressures.[23] According to their XRD study, more crystalline phases of CeO_2 were observed as the substrate temperature increased up to 500 °C. The tetravalent Ce with three different final states was observed in CeO_2 films by radio frequency magnetron sputtering method.[24]

Structural and spectroscopic investigations of Ce oxide nanofibers were very sparse to our knowledge. In this study, we fabricated Ce oxide nanofiber composites with different cerium concentrations applying sol-gel and the electrospinning process. The obtained nanofiber composites were calcined at 873 and 1173 K in order to manipulate the ratio of Ce(IV) to Ce(III) for obtaining the desired physical and chemical properties. And the synthesized cerium oxide nanofibers were characterized by scanning electron microscopy (SEM), X-ray diffraction (XRD), transmission electron microscopy (TEM), and X-ray photoelectron spectroscopy (XPS).

Experimental

Two different concentrations of Ce solutions were applied to fabricate Ce oxide nanofibers. The low concentration (denotes as CeL, 15.0 wt % of Ce) was obtained by dissolving 0.11 g of $Ce(NO_3)_3{\cdot}6H_2O$ and 0.62 g of polyvinylpyrrlidone (PVP) in the mixed solvent of 2 mL of distilled water and 10 mL of ethyl alcohol. And the solution was stirred for 12 hrs at room temperature. The high (CeH, 26.0 wt %) concentration of cerium nitrate solutions was made with 0.22 g of $Ce(NO_3)_3{\cdot}6H_2O$ powder. And other conditions were kept the same as the preparation of the CeL viscous solution. The viscosity of the solution was measured by using a viscometer (SV-10, A&D, Japan) and the viscosities of each solution were 65.1 and 68.7 cP for CeL and CeH,

respectively. Cerium(III) nitrate hexahydrate ($Ce(NO_3)_3 \cdot 6H_2O$, 99%) and PVP (MW: 1,300,000) were purchased from Aldrich. Ethyl alcohol (99.9% pure) was purchased from Burdick & Jackson.

In order to fabricate the Ce nanofibers, the viscous solutions were transferred into a 10 mL plastic syringe with a 22 gauge of metal needle and was delivered at a constant flow rate (15-16 μL/min) using a syringe pump (KDS scientific). The 0.41 kV/cm of electrical field was employed between the needle and a drum collector, which was covered with aluminum foil, to obtain Ce oxide nanofibers. The collector was rotating at a constant speed of 100 rpm. The obtained nanofiber composites were calcined at two different temperatures: 873 and 1173 K, which were chosen by the results of thermogravimetric analysis in our previous research.[27]

The morphology and the size of obtained nanofibers were determined by SEM (JEOL, JSM-6700F, Japan). In order to identify the crystal structure of the obtained nanofibers, XRD (PHILIPS, X'Pert-MPD, Netherlands) analysis was performed with 3 kW of Cu X-ray source. Data were collected from 10 to 80 degrees with a scanning speed of 3 degrees/min and the step size was 0.05°. TEM (JEOL, JEM-2010, Japan) analysis was performed to verify the crystallinity of the obtained nanofibers after calcining at 1173 K. The XPS (VG MultiLab 2000, UK) was carried out for investigation of the chemical nature of the Ce oxide nanofibers. The source of X-ray was Mg Kα (1253.6 eV) and the base pressure of XPS chamber was kept at around 1×10^{-10} Torr. The survey XP spectra were taken at 50 eV of constant analyzer energy (CAE) mode with 0.5 eV of energy step size. High resolution XP spectra such as Ce 3d, O 1s and C 1s were taken at 20 eV of CAE and 0.02 eV of energy step size. And other parameters were kept the same as the survey scan.

Result and Discussion

SEM Analysis. Figure 1 shows the SEM images of CeH and CeL nanofibers obtained at RT (denoted as CeH-RT and CeL-RT, respectively) after calcining at two different temperatures: 873 (CeH-873 and CeL-873) and 1173 K (CeH-1173 and CeL-1173). The surfaces of CeH-RT and CeL-RT were found to be smooth and uniform. After calcination was performed at 873 K, the rough surface of nanofibers was observed and the diameter had decreased. When the higher calcinations temperature (1173 K) was applied to the Ce nanofibers, small pores in the nanofibers

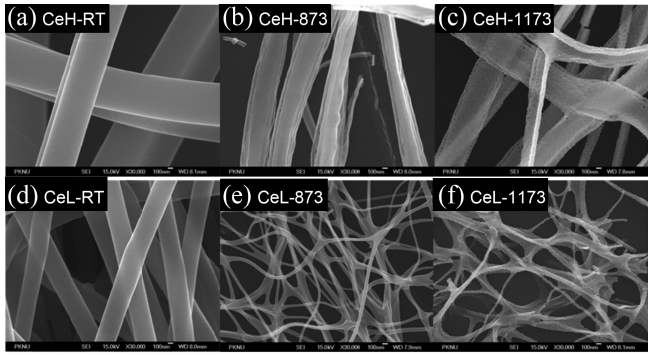

Figure 1. SEM images of PVP/$Ce(NO_3)_3$ nanofibers obtained at different calcination temperatures with different concentrations of cerium nitrate: CeL (15.0%) and CeH (26.0%).

formed. The decrease in diameter and the formation of pores are mainly due to the decomposition and removal of PVP and evaporation of water and nitrate group during calcination process. The diameter of CeL-1173 was decreased down to 13% of CeL-RT and nanofibers were stuck to form nano-sized mats. This implies that the composition ratio of PVP is greater than that of Ce in CeL-RT nanofibers. The diameter of CeH nanofibers, however, did not change as much as CeL reduced by increasing the calcination temperature. The Ce in CeH nanofibers might be a role as scaffolds of the nanofibers. It is worthy to note that the relative ratio of Ce to PVP was determined by the pathway of the formation of Ce oxide nanofibers. At low Ce ratio, the nanofibers diameter reduced remarkably because of the high composition of PVP which is decomposed and evaporated after calcinations. Pore formation was observed in CeH without reducing the diameter considerably because the high compositional ratio of Ce roles as backbone of the nanofiber. The measured mean diameters of Ce nanofibers are shown in Table 1. As the calcination temperature increased, the diameters of nanofibers decreased and/or pores formed.

XRD Analysis. The XRD patterns of the Ce oxide nanofibers obtained at RT and after calcination with various concentrations are shown in Figure 2. No peaks were observed from nanofibers at RT regardless of the concentration of cerium nitrate. This indicates that nanofibers obtained at RT by the electrospinning technique are amorphous.[27] After calcinations applied to the nanofibers, the cubic CeO_2 diffraction peaks appeared.[28] As the calcination temperature increased, more peaks evolved and the intensity increased as well. Comparing CeL and CeH, the more concentrated the

Table 1. Diameter and crystal size of CeL and CeH nanofibers with respect to different calcination temperature. Diameter was measured from SEM images and crystal size was obtained from XRD patterns using Scherrer's formula

		RT	873K	1173K
CeL	Diameter (nm)	375.03 (± 30.07)	54.68 (± 7.38)	47.20 (± 19.91)
	Crystal size (nm)	-	11.19	47.54
CeH	Diameter (nm)	741.08 (± 80.79)	382.42 (± 76.77)	611.61 (± 78.88)
	Crystal size (nm)	-	12.39	49.41

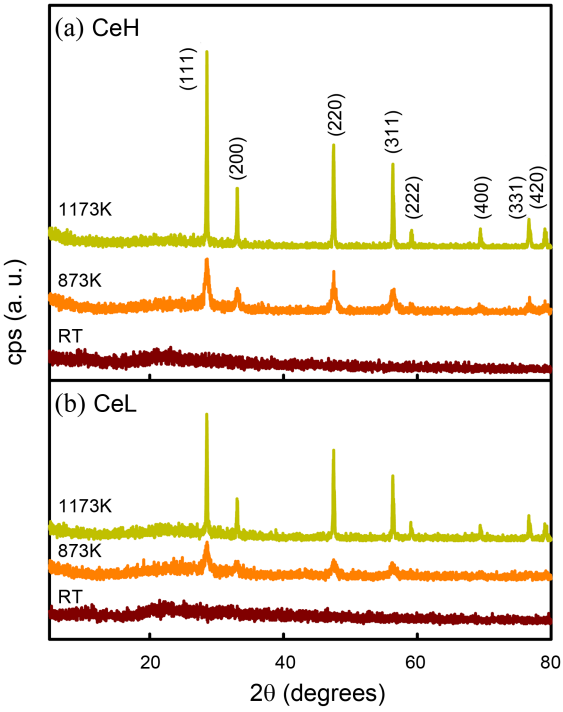

Figure 2. XRD patterns obtained from (a) CeH and (b) CeL nanofibers. All peaks present here are cubic CeO_2 peaks.

Ce solution was, the more evolved diffraction peaks were observed, which was expected. The crystal size of cubic CeO_2 obtained after calcining at 1173K was calculated by using Scherrer's formula, $D_p = (0.94\lambda)/(0.5\beta\cos\theta)$, where λ is the wavelength of X-ray source, β is the full width at the half maximum of a (111) peak, and θ is Bragg's diffraction angle. The obtained crystal size is shown in Table 1. The crystal size increased as the calcination temperature and the concentration of Ce increased.

TEM Analysis. The concrete crystallinity of Ce oxide nanofibers was examined with TEM and the images are shown in Figure 3. The ceria nanofibers were composed of nanoparticles with the average size of *ca.* 50 nm and nano-sized pores were observed as well shown in the insets. These small nanoparticles are mutually interconnected to form nanofibers and the resulted surface of Ce nanofiber was rough. Lattice patterns were observed and shown in upper parts of each image. The average lattice distances were measured with the Motic Images Plus 2.0ML program and the results are agrees with the reported values of d-spacing of cubic CeO_2 (111) plane.[29] Selected area electron diffraction (SAED) patterns of CeL-1173 and CeH-1173 nanofibers are shown at the bottom of each image. CeL-1173 showed spotty ring patterns indicating that polycrystalline fcc structure formed in CeL-1173. Clear fcc (001) pattern was observed at CeH-1173 with high crystallinity. The ratio of zone axes A/B was 1.4 which matched well with the theoretical value for fcc (001). These results are well cross supported with XRD data. As the amount of cerium increased in the nanofibers, more crystallinity was observed and the intensity of peaks increased.

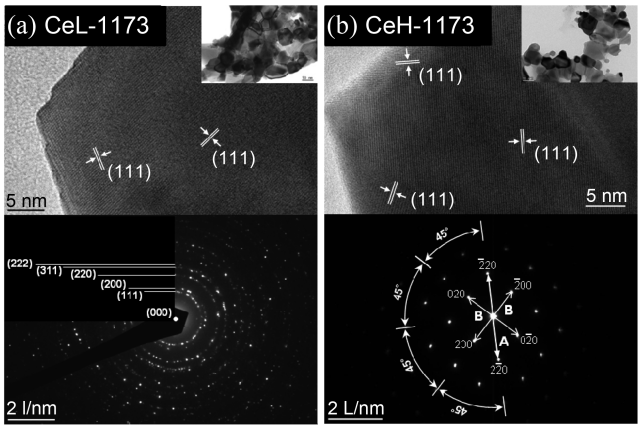

Figure 3. TEM images of (a) CeL-1173 and (b) CeH-1173 nanofibers. Top images show lattice pattern obtained from the insets of each image (scale bar = 50 nm) and the bottom images depict selected area diffraction patterns. Zone axes (A and B) are added in the bottom image of c) for clarity.

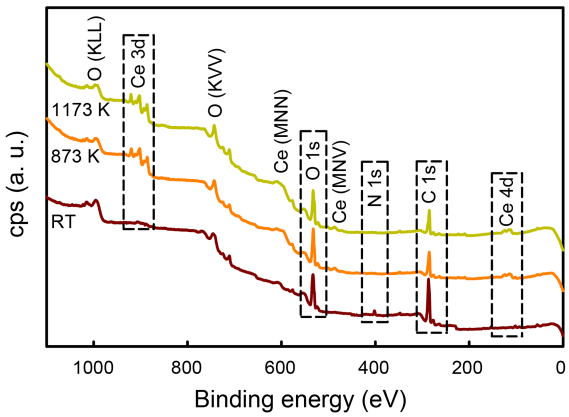

Figure 4. XP survey spectra of CeH nanofibers calcined at different temperatures.

XPS Analysis. The survey XP spectra of CeH nanofibers were shown in Figure 4. As the calcination temperature increased, Ce 3d and 4d peaks were pronounced. However the intensity of C 1s decreased and the N 1s peak was not detectable in CeH-873. The decomposition of PVP was confirmed by decreasing the intensity of C 1s and N 1s disappearing which were generated from PVP. Because of the decomposition of PVP, the ratio of Ce in calcined nanofibers was higher than that of CeH-RT. No other peaks except the peaks related with the elements in PVP and Ce are observed, so the feasibility of the fabrication of Ce oxide nanofibers by sol-gel and the electrospinning method is verified by XPS analysis.

More chemical information of C 1s and O 1s was obtained from high resolution XP spectra shown in Figure 5. In PVP, four chemically different carbons existed and were assigned as C1 (C=O), C2 (C-N), C3 (C-C=O), and C4 (C-C). These matched with 4 deconvoluted peaks of C 1s in CeH nanofibers from high to low binding energy. The atomic ratio of C1:C2:C3:C4 in PVP is 1:2:1:2. The atomic ratio in CeH-RT was almost the same as the ratio of pure PVP within experi-

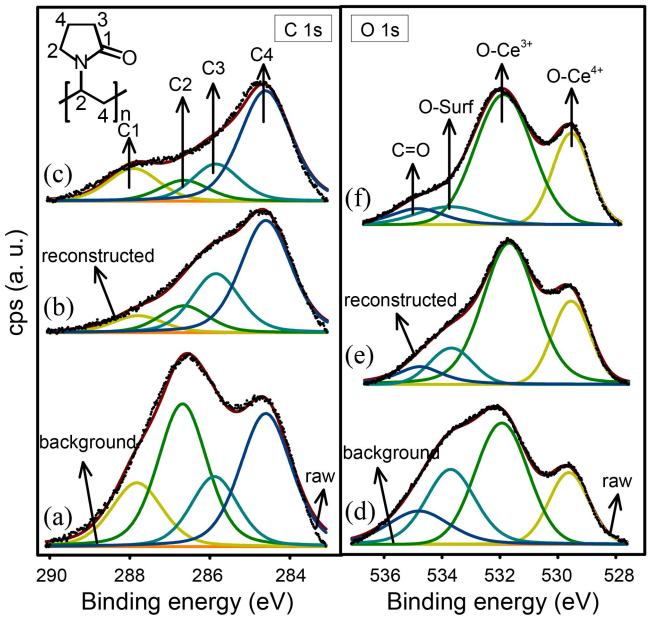

Figure 5. High resolution of XP spectra of C 1s and O 1s binding energy regions of CeH nanofibers; (a) and (d) for CeH-RT, (b) and (e) for CeH-873, and (c) and (f) for CeH-1173. The molecular structure of PVP is shown in upper side of C 1s spectra.

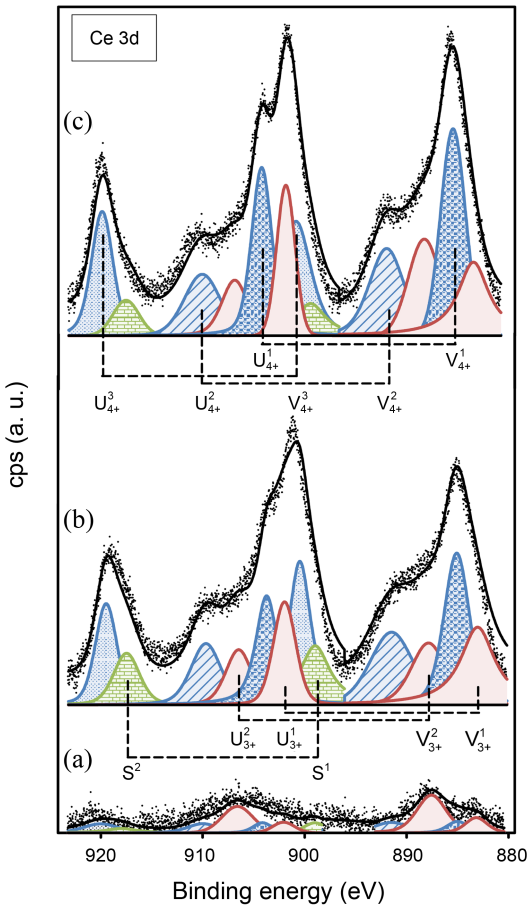

Figure 6. High resolution of XP spectra of Ce 3d binding energy regions of CeH nanofibers calcined at (a) RT, (b) 873 K, and (c) 1173 K. V is attributed to $3d_{5/2}$, U is attributed to $3d_{3/2}$ and S denotes satellite peak.

mental error. When the calcination temperature increased to 1173 K, C 1s peaks decreased due to the decomposition of PVP. Among them the intensity of C2 peak significantly decreased. This confirms that the decomposition of PVP progressed. The high resolution O 1s spectra of Ce oxide nanofibers were deconvoluted into four peaks: two oxygen species on the surface region (O-Surf.),[30,31] oxygen moieties bound with Ce^{3+} (O-Ce^{3+}) and Ce^{4+} (O-Ce^{4+}). In CeH-873, the amount of oxygen bound with Ce^{3+} and Ce^{4+} increased and that of surface oxygen decreased. Because the calcination causes the removal of surface oxygen, it is reasonable that the ratio of surface oxygen decreased. Further increase of calcination temperature, up to 1173 K, the portion of O-Ce^{4+} increased and the portion of O-Ce^{3+} decreased. Therefore it is highly possible that calcination of Ce oxide nanofibers at high temperatures led to oxidize Ce from Ce^{3+} to Ce^{4+}.

Figure 6 shows the deconvoluted high resolution XP spectra of Ce 3d region. Among the transition metal oxides, Ce oxide is one of the metal oxides which has various final states due to hybridization of Ce 4f and O 1s valence orbitals.[31,32] Ce has two characteristic oxidation states (+3 and +4). The Ce 3d core level spectra were deconvoluted to 3 doublet peaks for Ce^{3+} and Ce^{4+} each. The initial state of Ce^{3+} is $3d^{10}4f^1$ and that of Ce^{4+} is $3d^{10}4f^0$. Three final states were assigned for Ce^{3+} and Ce^{4+}species each. The deconvoluted 6 doublet peaks of Ce 3d spectra had a relatively similar spin-orbit splitting value of 18.65 ± 0.16 eV. In this paper, U and V notations are used for the assignment of Ce 3d corresponding to $3d_{3/2}$ and $3d_{5/2}$, respectively. The subscripts of U and V corresponds to the oxidation state of Ce and the superscripts are arbitrary numbers to differentiate the peaks of each oxidation state ordering from low to high binding energy. The detailed peak parameters and the final states of Ce oxide nanofibers are shown in Table 2. In the Ce^{3+} species, U^1_{3+}-V^1_{3+} are the shake down peaks, U^2_{3+}-V^2_{3+} are the main peaks, and S^1-S^2 are additional shake up

Table 2. The parameters applied for deconvolution of the Ce 3d XP spectra

	Ce^{3+}						Ce^{4+}					
Binding energy (eV)	883.7	902.5	888.4	907.2	899.7	918.2	885.8	904.6	892.2	910.2	901.2	920.2
Notation	V^1_{3+}	U^1_{3+}	V^2_{3+}	U^2_{3+}	S^1	S^2	V^1_{4+}	U^1_{4+}	V^2_{4+}	U^2_{4+}	V^3_{4+}	U^3_{4+}
Initial state	$Ce\ 3d^{10}4f^1$-$O\ 2p^6$						$Ce\ 3d^{10}4f^0$-$O\ 2p^6$					
Final state	$Ce\ 3d^94f^2$-$O\ 2p^5$		$Ce\ 3d^94f^1$-$O\ 2p^6$		-		$Ce\ 3d^94f^2$-$O\ 2p^4$		$Ce\ 3d^94f^1$-$O\ 2p^5$		$Ce\ 3d^94f^1$-$O\ 2p^6$	

satellite peaks adapted to fitting the raw data.[32] In the Ce^{4+} moiety, two shake down peaks (U^1_{4+}-V^1_{4+} and U^2_{4+}-V^2_{4+}) were assigned and the main peaks (U^3_{4+}-V^3_{4+}) were the characteristic peaks of Ce^{4+}. In CeH-RT, both Ce^{3+} and Ce^{4+} features were detected in Ce 3d spectrum and Ce^{3+} was dominated. After Ce oxide nanofibers were calcined at 873 K, the amount of Ce^{3+} and Ce^{4+} both increased remarkably. This phenomenon strongly supports the results observed in C 1s XP spectra that the decomposition of PVP occurred at 873 K. However, predominant features changed to Ce^{4+}. Further increase of calcination temperature to 1173 K, showed us that the amount of Ce^{3+} decreased, while Ce^{4+} increased. This result indicates that the oxidation of Ce from +3 to +4 occurred during calcination of Ce oxide nanofibers. This behavior is also confirmed by O 1s spectra in Figure 5.

Conclusion

PVP/$Ce(NO_3)_3$ composite nanofibers were successfully fabricated by using sol-gel and the electrospinning technique. And Ce oxide nanofibers were synthesized by calcining the composite nanofibers at 873 and 1173 K. SEM images indicated that the diameter of CeO_2 nanofibers decreased by increasing calcination temperature. As the amount of cerium increased, diameter of CeO_2 nanofibers increased. XRD analysis revealed that the PVP/$Ce(NO_3)_3$ nanofibers were amorphous and cubic CeO_2 nanofibers formed after calcining at 873 K. As the calcination temperature increased, the crystal size of Ce_2O increased. The peak intensity increased with increase of the cerium nitrate concentration. TEM results revealed that the Ce oxide nanofibers were composed with nanoparticles. And spotty ring patterns (CeL) indicated that the Ce oxide nanofibers were of a polycrystalline structure. And CeH diffraction pattern is fcc. XPS study indicated that as the calcination temperature increased, Ce 3d peak evolved by removal of PVP at CeH-873. Further increase of calcination temperature resulted that the oxidation state of Ce shifted from Ce^{3+} to Ce^{4+}. XP spectra of Ce 3d and O 1s revealed that the oxidation of Ce occurred during calcination of Ce nanofibers.

Acknowledgments. This research was supported by Basic Science Research Program through the National Research Foundation of Korea (NRF) funded by the Ministry of Education, Science and Technology (2010-0021332). The author YCK acknowledged to Jisoo Kang for proofreading.

References

1. Ashammakhi, N.; Ndreu, A.; Piras, A. M.; Nikkola, L.; Sindelar, T.; Ylikauppila, H.; Harlin, A.; Gomes, M. E.; Neves, N. M.; Chiellini, E.; Chiellini, F.; Hasirci, V.; Redl, H.; Reis, R. L. *J. Nanosci. Nanotechnol.* **2007**, *7*, 862.
2. Yang, A.; Tao, X.; Pang, G. K. H.; Siu, K. G. G. *J. Am. Ceram. Soc.* **2008**, *91*, 257.
3. Chen, S.; Hau, H.; Hu, P.; Wendorff, J. H.; Greiner, A.; Agarwal, S. *Macromol. Mater. Eng.* **2009**, *294*, 781.
4. Chuangchote, S.; Supaphol, P. *J. Nanosci. Nanotechnol.* **2006**, *6*, 125.
5. Luepong, K.; Koombhongse, P.; Kongkachuichay, P. *Chiang Mai J. Sci.* **2009**, *37*(1), 85.
6. Kang, M. S.; Jin, H. J. *Key Engineering Materials* **2006**, *321*, 934.
7. Bolgen, N.; Menceloglu, Y. Z.; Acatay, K.; Vargel, I.; Piskin, E. *J. Biomater. Sci. Polymer Edn.* **2005**, *16*, 1537.
8. Stasiak, M.; Roben, C.; Rosenberger, N.; Schleth, F.; Studer, A.; Greiner, A.; Wendorff, J. H. *Polymer* **2007**, *48*, 5208.
9. Stasiak, M.; Studer, A.; Greiner, A.; Wendorff, J. H. *Eur. J. Inorg. Chem*. **2007**, *13*, 6150.
10. Kim, S. J.; Nam, Y. S.; Rhee, D. M.; Park, H. S.; Park, W. H. *European Polymer Journal* **2007**, *43*, 3146.
11. Caricato, A. P.; Capone, S.; Ciccarella, G.; Martino, M.; Rella, R.; Romano, F.; Spadavecchia, J.; Taurino, A.; Tunno, T.; Valerini, D. *Applied Surface Science* **2007**, *253*, 7937.
12. Wang, Y.; Yang, Q.; Shan, G.; Wang, C.; Du, J.; Wang, S.; Li, Y.; Chen, X.; Jing, X.; Wei, Y. *Materials Letter* **2005**, *59*, 3046.
13. Maze, B.; Vahedi Tafreshi, H.; Wang, Q.; Pourdeyhimi, B. *Aerosol Science* **2007**, *38*, 550.
14. Gopal, R.; Kaur, S.; Ma, Z.; Chan, C.; Ramakrishna, S.; Matsuura, T. *J. Memb. Sci.* **2007**, *281*, 581.
15. Ramaseshan, R.; Sundarrajan, S.; Jose, R.; Ramakrishna, S. *J. Appl. Phys.* **2007**, *102*, 111101
16. Namai, Y.; Fukui, K. I.; Iwasawa, Y. *J. Phys. Chem. B* **2003**, *107*, 11666.
17. Barreca, D.; Gasparotto, A.; Tondello, E.; Sada, C.; Polizzi, S.; Benedetti, A. *Chem. Vap. Depos.* **2003**, *9*, 199.
18. Muroga, T.; Iwai, H.; Yamada, Y.; Izumi, T.; Shiohara, Y.; Iijima, Y.; Saito, T.; Kato, T.; Sugawara, Y.; Hirayama, T. *Physica. C* **2003**, *796*, 392.
19. Shirakawa, M.; Unno, J.; Aizawa, K.; Kusunoki, M.; Mukaida, M.; Ohshima, S. *Physica. C* **2003**, *1346*, 392.
20. Kleinlogel, C.; Gauckler, L. J. *Adv. Mater.* **2001**, *13*, 1081.
21. Kendall, K.; Palin, M. *J. Power Sources* **1998**, *71*, 268.
22. Patsalas, P.; Logothetidis, S.; Metaxa, C. *Appl. Phys. Lett.* **2002**, *81*, 466.
23. Kanakaraju, S.; Mohan, S.; Sood, A. K. *Thin Solid Films* **1997**, *305*, 191.
24. Guo, S.; Arwin, H.; Jacobson, S. N.; Jarrendahl, K.; Helmerson, U. *J. Appl. Phys.* **1995**, *77*, 5369.
25. Sohlberg, K.; Pantelides, S. T.; Pennycook, S. J. *J. Am. Chem. Soc.* **2001**, *123*, 6609.
26. Yang, X.; Shao, C.; Liu, Y.; Mu, R.; Guan, H. *Thin Solid Films* **2005**, *478*, 228.
27. Qizheng, C.; Xiangting, D.; Jinxian, W.; Mei, L. *Journal of Rare Earths* **2008**, *26*, 664.
28. JCPDS Database, International Center for Diffraction Data 1997, PDF 81-0792.
29. Kang, M.; Park, E. D.; Kim, J. M.; Yie, J. E. *Appl. Catal. A* **2007**, *327*, 261.
30. Yao, H. B.; Li, Y.; Wee, A. T. S. *Appl. Surf. Sci.* **2000**, *158*, 112.
31. Sohal, R.; Lupina, G.; Seifarth, O.; Zaumseil, P.; Walczyk, C.; Schroeder, T. *Surf. Sci.* **2010**, *604*, 276.
32. Bera, S.; Mittal, V. K.; Venkata Krishnan, R.; Saravanan, T.; Velmurugan, S.; Nagarajan, K.; Narasimhan, S. V. *J. Nucl. Mat.* **2009**, *393*, 120.